Supporting Information

Giavazzi et al. 10.1073/pnas.1214589110

SI Materials and Methods

Raw Data Conversion. The sensor surface is modeled as a planar interface between two transparent media with refractive indexes of n_1 (substrate) and n_2 (aqueous solution). The composite molecular layer formed of the copolymer coating, the immobilized probes, and the bound targets is modeled as a uniform, transparent thin slab with a thickness of h, an average density of ρ, and an average refractive index of n_L. The reflectivity (R) of a portion of the surface illuminated by a collimated beam with a wavelength of λ can be calculated by means of thin-film Fresnel formulas (1). In the case that $h << \lambda$, as the refractive indexes of the substrate and solution are very close (typically $|n_2 - n_1| < 10^{-2}$), the value of R can be well approximated by

$$R \cong R_0 + (2r_{1L}\alpha)^2, \qquad \textbf{[S1]}$$

where $\alpha = 2\pi h n_L \cos(\theta_L)/\lambda$ is the phase shift between the rays reflected from the two sides of the film, θ_L is the angle between the ray transmitted in the film and the surface normal, R_0 is the reflectivity of the bare surface, and r_{1L} is the reflection coefficient of the substrate/film interface. Eq. **S1** can be written in terms of the surface density (σ) of the thin layer by means of the substitution $h = \sigma/\rho$, thus obtaining the expression (Eq. **1** of the main text)

$$\frac{\sigma(t)}{\sigma_0} = \sqrt{\frac{u(t)}{u_0} - 1}, \qquad \textbf{[S2]}$$

where $u(t)$ and u_0 are the brightness measured for the considered pixel and from the bare surface, respectively, and the value of σ_0 is given by

$$\sigma_0 = \frac{\rho\lambda\sqrt{R_0}}{4\pi n_L r_{1L}\cos(\vartheta_L)}. \qquad \textbf{[S3]}$$

The surface density of the spotted surface measured in incubation buffer and bovine serum is calculated using the following set of parameters (yielding $\sigma_0 = 4.9$ ng/mm^2): $\lambda = 636$ nm, $\theta_L = 41.4°$, $n_1 = 1.327$, $n_2 = 1.335$, $n_L = 1.42$, and $\rho = 1.1$ g/cm^3 (where the values of n_L and ρ are obtained from ref. 2). In the case of the copolymer coating layer surrounding the spots, the value of $\sigma_0 = 1.9$ ng/mm^2 is obtained, assuming $n_L = 1.36$ and $\rho = 0.15$ g/cm^3, according to ref. 3.

Fitting of the Binding Curves Measured in the Presence of Serum. As shown in Fig. 2*B*, the addition of bovine fetal serum in the RPI measuring cuvette to a final dilution of 1:10 yielded a limited and rather slow increase of reflectivity due to the nonspecific adsorption of serum components on the sensing surface. Fig. S1 reports the data of Fig. 2*B* corresponding to the sole nonspecific adsorption of serum (Fig. S1*A*) and to the processes due to the subsequent addition of the antigens, p24 capsid protein (p24Ag) and hepatitis B surface antigen (HBsAg) (Fig. S1 *B* and *C*). The $\Delta\sigma/\sigma_0$ data of Fig. S1*A* are well fitted by stretched exponentials (black lines) with values of the stretching exponents of 0.40, 0.48, 0.51, and 0.69 for the spots of antibodies targeting p24Ag [p24(d)Ab], anti-β-Lactoglobulin (CTR1), antibodies targeting HBsAg [HBs(c)Ab] and antibodies recognizing Toxoplasma gondii antigens (CTR2), respectively. The high quality of the fits and the obtained values of the stretched exponents support the notion of a variety of interactions contributing to the adsorption process with different kinetics.

The subsequent addition of p24Ag and HBsAg in the serum solution produced a further increase of the $\Delta\sigma/\sigma_0$ signal measured from the p24(d)Ab and HBs(c)Ab spots, which added to the nonspecific adsorption process of serum. To properly separate the binding process from the adsorption of serum components, the estimated signal from serum adsorption can be subtracted from the $\Delta\sigma/\sigma_0$ curves measured in the presence of antigen binding by using the stretched-exponential functions extracted from the previous fits. Alternatively, a more approximate but potentially more practical approach can be followed: The signal from suitable control spots not interacting with the antigens can be used as references and subtracted from the measured binding curves. Fig. S1 *B* and *C* shows that, although the nonspecific adsorption of serum on control spots CTR1 and CTR2 slightly differs from that of p24(d)Ab and HBs(c)Ab spots, respectively, the two approaches lead to very similar results. The obtained binding curves are all well fitted by single exponential functions with rates differing by less than 10% for the two approaches, being 4.1×10^{-4} s^{-1} and 4.5×10^{-4} s^{-1} for p24(d)Ab and 5.6×10^{-5} s^{-1} and 5.8×10^{-5} s^{-1} for HBs(c)Ab, the rates extracted after subtraction of the corresponding stretched-exponential function (green open circles in Fig. S1*B* and red open circles in Fig. S1*C*) and after subtraction of the corresponding control spot signal (cyan circles in Fig. S1*B* and magenta circles in Fig. S1*C*), respectively. The validity of the single exponential fits is also confirmed by repeating the fitting with stretched-exponential functions. The obtained values of stretched exponent for the curves in Fig. S1 *B* and *C* are 1 ± 0.05 and the fitting curves are substantially identical to those obtained by single exponential fits, hence confirming the single exponential shape of the binding curves.

Kinetic and Equilibrium Analysis of p24(c)Ab/p24Ag Interaction by Reflective Phantom Interface. The experiment reported in Fig. 3 *A–E* was repeated also for the interaction between p24Ag and p24(c)Ab antibodies, providing independent estimates of the extracted kinetic and equilibrium parameters. We measured the binding of p24Ag on a single spot of p24(c)Ab as increasing quantities of the antigen were progressively added to the cuvette containing the incubation buffer. The results of this study are reported in Fig. S2. Fig. S2*A* shows the relative reflectivity of a single spot of p24(c)Ab antibodies measured after the addition of p24Ag in buffer, from 3 to 130 ng/mL. Fig. S2*B* reports the data of Fig. S2*A* after conversion into bound surface mass by means of Eq. **1**. The red lines are the exponential fittings to the curves. In Fig. S2*C*, the rates of the exponential fits reported in Fig. S2*B* are shown as a function of the target concentration (blue squares) and are fitted by $\Gamma(c) = k_{on}c + k_{off}$ (red line), yielding $k_{on} = 6.5 \times 10^5$ ($\pm 1 \times 10^5$) M^{-1}·s^{-1} and $k_{off} = 1.2 \times 10^{-4}$ ($\pm 3 \times 10^{-5}$) s^{-1}. In Fig. S2*D*, the asymptotic values extracted from the exponential fits reported in Fig. S2*B* are shown as function of the target concentration (blue squares) and are fitted, according to Eq. **2**, by $\Delta\sigma/\sigma_0 = (\Delta\sigma_{max}/\sigma_0)/(1 + K_d/c)$ (red line), where $K_d = 0.6$ (± 2) nM. An independent measure of k_{off} is also obtained monitoring the reflectivity decrease as a function of time after replacing the target solution with the incubation buffer (Fig. S2*E*). The red line represents an exponential fit yielding a k_{off} of 1.2×10^{-4} ($\pm 2 \times 10^{-5}$) s^{-1}, in remarkable agreement with the value obtained from the fit of the $\Gamma(c)$ dependence.

Binding Curves Measured by Reflective Phantom Interface and Corresponding Exponential Fits. The binding curves measured by the reflective phantom interface (RPI) method for different spots of differently functionalized sensing surfaces are reported in Figs. S3–S5, together with their exponential fits, from which the rates reported in Figs. 3 *F* and *G* (orange down triangles and open red circles) and 4 are obtained. The asymptotic plateau of the curves at the lowest concentrations is inferred by the concentration dependence of the plateaus of the highest concentration curves, according to the equilibrium solution of Eq. **2**, $\Delta\sigma/\sigma_0 = (\Delta\sigma_{max}/\sigma_0)/(1 + K_d/c)$, from which an estimate of the dissociation equilibrium constant K_d is obtained. This procedure enables one to determine the values of $\Gamma(c) = k_{on}c + k_{off}$ over the considered concentration range. The extracted kinetic parameters are reported in Table 1.

Characterization of p24(d)Ab and HBs(c)Ab by Surface Plasmon Resonance. Surface plasmon resonance (SPR) measurements were performed on a BIAcore X100 instrument (GE-Healthcare), using research-grade CM5 or CM3 carboxyl-methyl-dextran–coated sensorchips (GE-Healthcare). The sensorchips were activated for 7 min at a flow rate of 10 μL/min, using a 1:1 ratio of 0.4 M 1-ethyl-3-(3-dimethylpropyl) carbodiimide and 0.1 M *N*-hydroxysucciminide, the ligands immobilized by amine coupling (see below for further details) and the excess activated groups blocked by a 7-min injection at 30 μL/min of 1 M ethanolamine, pH 8.5. To minimize mass transport effects, preliminary experiments were performed to select a low density of immobilized antibodies that still retains the capacity to report a reliable binding of the corresponding antigen.

For the study of its interaction with p24Ag, p24(d)Ab [50 μg/mL in 10 mM Hepes buffer pH 7.4 containing 150 mM NaCl, 3 mM EDTA, and 0.005% surfactant P20 (HBS-EP)] was injected onto the CM5 sensorchip, allowing the immobilization of 1,130 resonance units (RU) equal to 7.5 fmol/mm^2 of the antibody. Instead, for the study of its interaction with HBsAg, HBs(c)Ab was injected onto the CM3 sensorchip (5 μg/mL in HBS-EP), allowing the immobilization of 2,000 RU equal to 13.3 fmol/mm^2 of the antibody. Void deactivated CM5 or CM3 sensorchips were used to evaluate nonspecific bindings and for blank subtractions. Increasing concentrations of p24Ag or HBsAg in HBS-EP buffer were injected at 30 μL/min for 2 min to allow their association to the respective antibodies and then washed for 10 min to allow their dissociation. Kinetic parameters were calculated by BIAcore X100 evaluation software, version 2.0.1. As shown in Fig. S6, p24Ag binds in a dose-dependent manner to immobilized p24(d)Ab and, after its association, it spontaneously dissociates from the sensorchip. The k_{on} and k_{off} rates calculated in two separate analyses were equal to $5.0 \pm 0.14 \times 10^4$ [1/(sM)] and $1.7 \pm 0.97 \times 10^{-4}$ (1/s), respectively. The dissociation constant (K_d) calculated as k_{off}/k_{on} was then equal to 3.2 ± 1.2 nM. To address the possible limitations due to mass transport, we estimated the largest association rate for which this kind of limitation can be neglected according to ref. 4. The extrapolated plateau of the signal due to p24Ag saturation is 250 RU, corresponding to a surface density of 10.4×10^{-10} M*cm for a 24-kDa protein. Considering a flow rate of 30 μL/min and the size of the measuring channel, it is derived that the mass transport limitation can be neglected for rates below 1.7×10^6 1/(sM), a value much larger than the rates measured in the reported experiments.

Preliminary experiments showed that HBsAg irreversibly binds to the HBs(c)Ab antibodies on the surface. We tested several potential regeneration conditions (acidic, basic, and high salt) to detach HBsAg from HBs(c)Ab that turned out, however, to be inefficient, causing instead a reduced antibody activity in subsequent analyses. The irreversible nature of the HBsAg interaction cannot be ascribed to general problems of the SPR analyses, such as nonspecific binding, as sustained by the absence of HBsAg binding to the control surface (Fig. S7*A*). More likely, it is possibly due to the tendency of HBsAg to aggregate (as discussed in the main text), possibly gaining a multivalent binding capability that may entrap the antigen in the tridimensional mesh of antibodies immobilized on the CM3 surface and interfere with the process of dissociation. Whatever its cause, the irreversible HBsAg binding to sensorchip-immobilized antibody forced us to perform the analysis in a single-cycle mode (5, 6). Briefly, in this model the antigen is injected at increasing concentrations within a single scan and without surface regeneration between injections. Important to note, both the multi- and the single-cycle modes have been demonstrated to provide very similar kinetic rate constants (5, 6). As shown in Fig. S7*B*, HBsAg binds HBs(c)Ab antibody in a dose-dependent and irreversible manner, allowing the calculation only of the k_{on}. Two separate analyses provided a mean value for this parameter equal to $0.5 \pm 0.02 \times 10^4$ [1/(sM)].

SPR Detection of Nonspecific Serum Adsorption. To evaluate the effect of serum on the copolymer coating used with the RPI method, we compared the extent of nonspecific binding occurring on a SPR gold surface coated with the copolymer of dimethylacrylamide (DMA), *N*-acryloyloxysuccinimide (NAS), and 3-(trimethoxysilyl) propyl methacrylate (MAPS) [copoly(DMA-NAS-MAPS)] or with the widely used carboxyl-methyl-dextran. We performed repeated injections of serum onto the two surfaces, calculating the amount of material that remains adsorbed after extensive washes. In detail, SPR measurements were performed on a BIAcore X100 instrument (GE-Healthcare), using research-grade CM5 or a gold-coated sensorchip for SPR analysis (Xantech Bioanalytics) on which the copolymer was coated. Both the sensorchips were de-activated by a 7-min injection at 30 μL/min of 1 M ethanolamine, pH 8.5. The sensorchips were then saturated by an overnight flux at 5 μL/min of 1% BSA diluted in 0.05 M Tris·HCl (pH 7.6), 150 mM NaCl, and 0.02% Tween 20 (running buffer). One hundred microliters of fetal bovine serum (FBS) 1:10 in running buffer was injected at 30 μL/min onto the sensorchips. The injections were repeated 5 and 6 times for both the copolymer-coated chip and the CM5 sensorchips, with extensive washes (30–50 min at 5 μL/min) with running buffer to allow the dissociation of the adsorbed material. As shown in Fig. S8*A*, the amount of serum components that remain nonspecifically bound to the sensorchip coated with the copolymer is remarkably low (5–39 RU) and decreases after each injection. In the same experimental conditions, the amount of serum components that remain adsorbed to the CM5 sensorchip can be even 10 times higher (11–396 RU). Also in this case a decrease of the nonspecific binding is observed following repeated injections (Fig. S8*B*).

Dual Polarization Interferometry Quantification of Nonspecific Serum Adsorption. Farfield dual polarization interferometry (DPI) technology provides a tool to monitor the surface adsorption and desorption of molecules on a surface (7). DPI measurements were carried out to investigate the effects of serum on the copoly (DMA-NAS-MAPS) coating. The data were obtained using an Analight Bio 200 (Farfield Group), and the sensing surface was a silicon oxynitride AnaChipTM. The coating procedure was the same as for the fluoropolymer substrate. The unreacted succinimide esters were blocked by incubation of the coated chips in 50 mM ethanolamine, 50 mM Tris·HCl, pH 9. The coated sensor chip was assembled into the instrument and flushed using the incubation buffer as a running buffer; this precondition was carried out for several hours at a flow rate of 5 μL/mL. Five injections of 40 min of serum diluted in incubation buffer (1:10) were performed. Each injection was followed by a wash with incubation buffer and the mass adsorbed on the surface was then estimated (Fig. S8*C*). The data were analyzed using the Analight Explorer software. The amount of nonspecific binding was consistent with that observed on the copolymer-coated Hyflon AD surface.

Effect of the Stirring Speed on the Binding Rates Measured by RPI. The dependence on the stirring bar rotational speed of the measured binding rates of p24Ag on p24(d)Ab and p24(c)Ab spots was measured as shown in Fig. S9. The stirring speed was changed every 5 min after the addition of p24Ag, alternating fast and slow speeds in a range between 111.8 and 213.8 rad/s. Remarkably, the effect of the changes of the rotational speed on the slope of the measured binding curve was very limited. Fig. S9*B* displays a magnification of the binding curve showing the small difference between the slopes of the curve fragments measured at different stirring speeds (fitted by the blue line) relative to the fit of the whole curve (fitted by the red line). In Fig. S9*C* the measured rates are reported as a function of the rotational speed for the two p24 antibodies. In the case of p24(d)Ab (blue squares), which displays a faster binding kinetic, the observed rates exhibit a small tendency to increase as a function of the rotational speed, whereas the rates for p24(c)Ab (green circles) do not show a clear dependence.

To evaluate the transport efficiency of the mixing method here used, it should be considered that at the highest rotational speeds the fluid dynamics are dominated by turbulence, as is also clearly visible by direct inspection. Indeed, considering a stirred vessel geometry (8), for the range of rotation speed values explored in Fig. S9, the value of the Reynolds number is expected to be in the range $Re = 0.5–1.5 \times 10^4$, whereas the limit for laminar flow is $Re < 10$ and a fully developed turbulence should occur for $Re > 10^4$. In these conditions and for the particular geometry of the inner volume of the cuvette, the detailed theoretical dependence of the measuring rates on the rotational speed is not known, although highly enhanced mixing capabilities are expected for the highest speed relative to the lowest because of the occurrence of turbulent dynamics, which is expected to highly increase the local transport efficiency on the sensing surface. Therefore, the small dependence of the measured rates on the rotational speed of the stirrer shown in Fig. S9*C* suggests substantially negligible mass transport limitations. This observation is also supported by the comparison of the rates measured with SPR, which are similar to those obtained by RPI for HBs(c)Ab and even slightly slower in the case of p24(d)Ab (Table 1).

1. Pedrotti FL, Pedrotti LS (1993) *Introduction to Optics* (Prentice Hall, Upper Saddle River, NJ), 2nd Ed, pp 392–396.
2. Vörös J (2004) The density and refractive index of adsorbing protein layers. *Biophys J* 87(1):553–561.
3. Yalçin A, et al. (2009) Direct observation of conformation of a polymeric coating with implications in microarray applications. *Anal Chem* 81(2):625–630.
4. Goldstein B, Coombs D, He X, Pineda AR, Wofsy C (1999) The influence of transport on the kinetics of binding to surface receptors: Application to cells and BIAcore. *J Mol Recognit* 12(5):293–299.
5. Karlsson R, Katsamba PS, Nordin H, Pol E, Myszka DG (2006) Analyzing a kinetic titration series using affinity biosensors. *Anal Biochem* 349(1):136–147.
6. Trutnau HH (2006) New multi-step kinetics using common affinity biosensors saves time and sample at full access to kinetics and concentration. *J Biotechnol* 124(1): 191–195.
7. Swann MJ, Peel LL, Carrington S, Freeman NJ (2004) Dual-polarization interferometry: An analytical technique to measure changes in protein structure in real time, to determine the stoichiometry of binding events, and to differentiate between specific and nonspecific interactions. *Anal Biochem* 329(2):190–198.
8. Bittorf K, Kresta S (2000) Limits of fully turbulent flow in a stirred tank. *Proceedings of the 10th European Conference on Mixing*, eds van den Akker HEA, Derkse JJ (Elsevier Science, Amsterdam) pp 17–24.

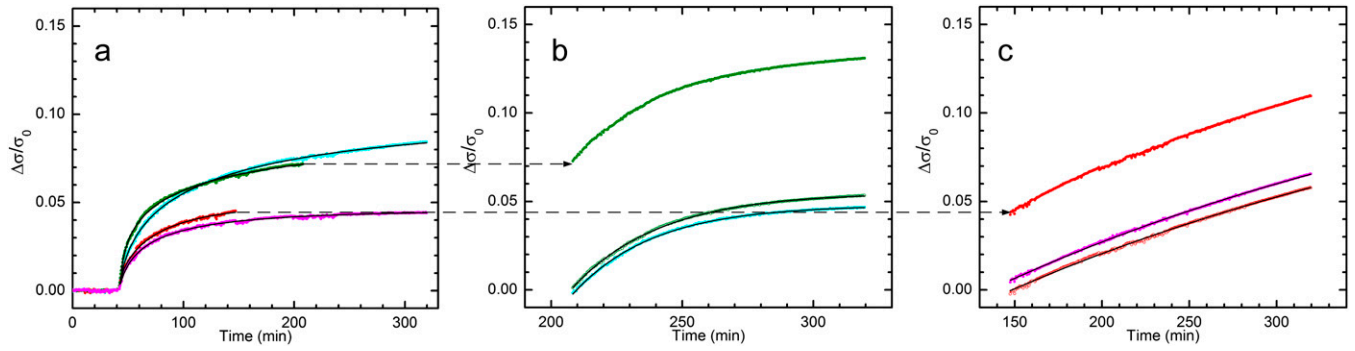

Fig. S1. Kinetics of nonspecific adsorption of serum components and of specific binding in the presence of serum. (*A*) Adhering normalized mass on single spots of HBs(c)Ab (red) and p24(d)Ab (green) antibodies and on control spots, CTR1 (cyan) and CTR2 (magenta), after the addition of 1:10 dilution of bovine fetal serum. The black curves are stretched-exponential fits (*SI Materials and Methods*). (*B*) Mass adhering on a spot of p24(d)Ab after the addition of p24Ag in serum reported on the same $\Delta\sigma/\sigma_0$ scale as in *A* (green solid circles), after the subtraction of the stretched-exponential function fitting the data of *A* for the same spot (green open circles) and after subtraction of the CTR1 data of *A* (cyan). The black curves are single exponential fits (*SI Materials and Methods*). (*C*) Mass adhering on a spot of HBs(d)Ab after the addition of HBsAg in serum reported on the same $\Delta\sigma/\sigma_0$ scale as in *A* (red solid circles), after the subtraction of the stretched-exponential function fitting the data of *A* for the same spot (red open circles) and after subtraction of the CTR2 data of *A* (magenta).

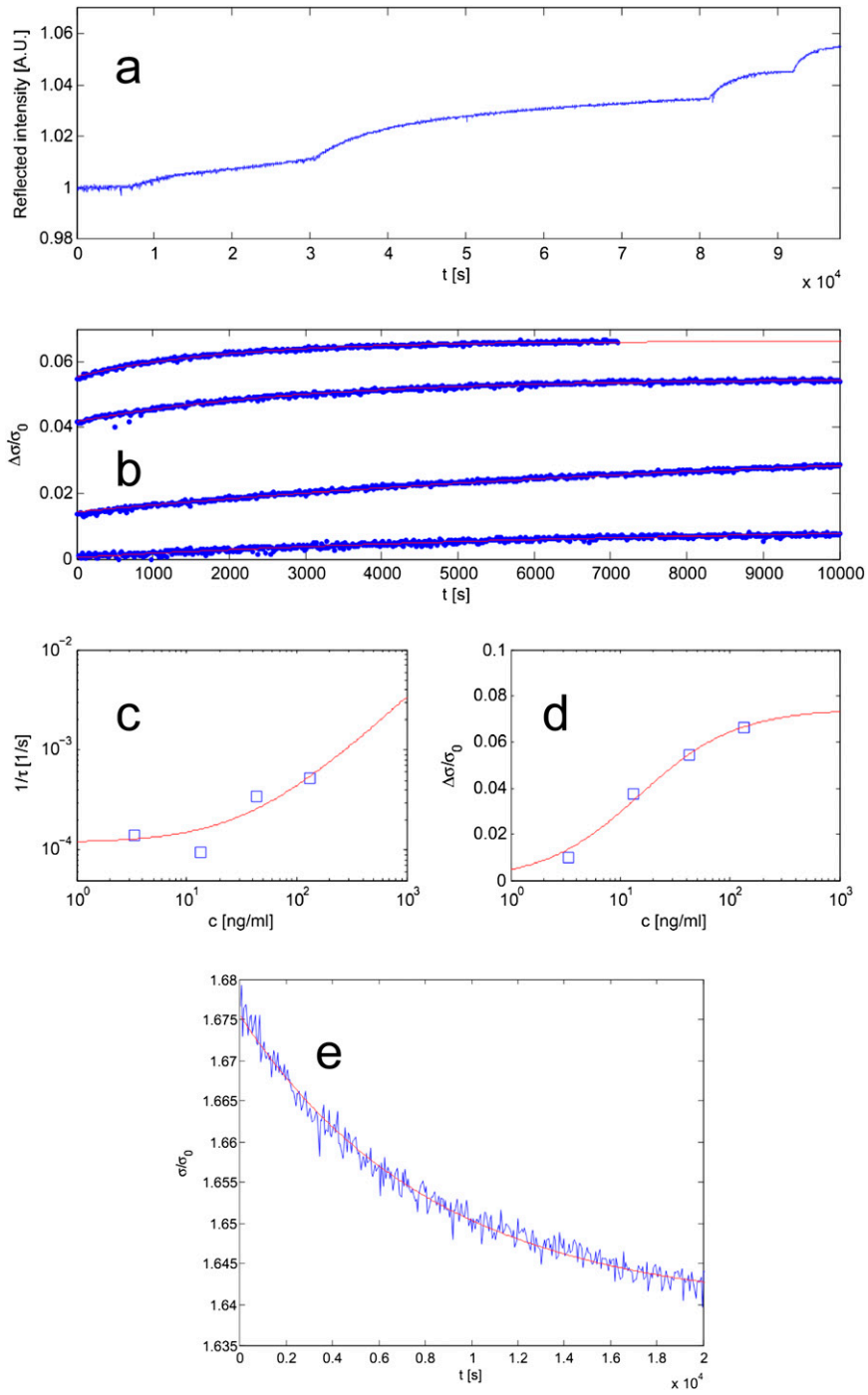

Fig. S2. Kinetic and equilibrium analysis of p24(c)Ab/p24Ag interaction measured by RPI. (*A*) The time dependence of the reflected intensity of a single spot of p24(c)Ab antibodies was measured while the solution concentration of target protein was brought to 3.4, 13.3, 43.1, and 133 ng/mL. (*B*) The curves in *A* are converted into the normalized mass of target molecules adhering to the spot and reported as a function of the time after each addition (blue circles) together with their exponential fits (red lines). (*C*) The rates of the exponential fits reported in *B* are shown as a function of the target concentration (blue squares) and are fitted by $\Gamma(c) = k_{on}c + k_{off}$ (red line), yielding $k_{on} = 6.5 \times 10^5\ M^{-1}{\cdot}s^{-1}$ and $k_{off} = 1.2 \times 10^{-4}\ s^{-1}$. (*D*) The asymptotic values extracted from the exponential fits reported in *B* are shown as a function of the target concentration (blue squares) and are fitted, according to Eq. **2**, by $\Delta\sigma/\sigma_0 = (\Delta\sigma_{max}/\sigma_0)/(1 + K_d/c)$ (red line), where $K_d = 0.6$ nM. (*E*) A dissociation curve is measured, replacing the target solution with the incubation buffer. The red line represents an exponential fit yielding a k_{off} of $1.2 \times 10^{-4}\ s^{-1}$.

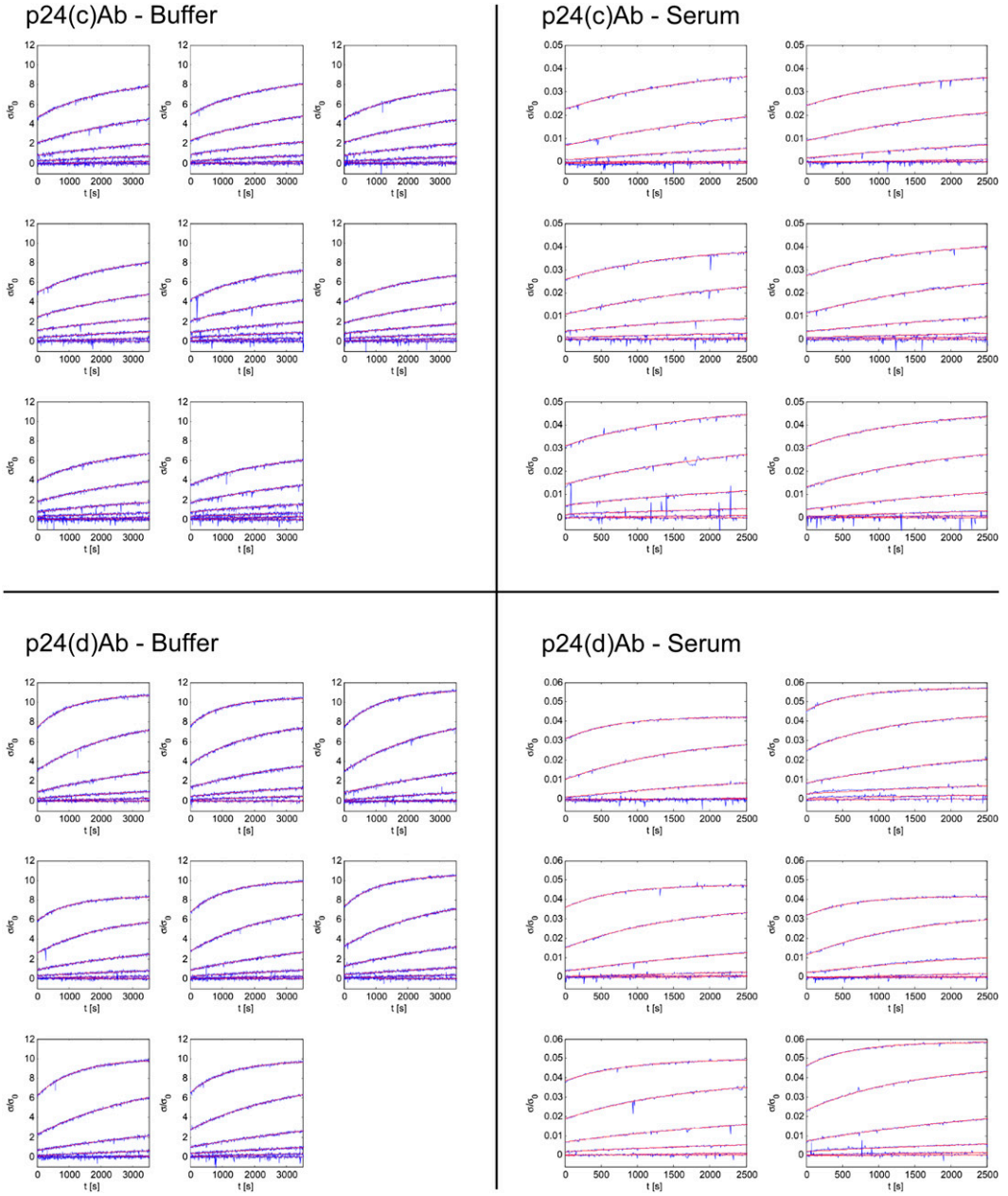

Fig. S3. Binding curves of p24Ag on p24(c)Ab and p24(d)Ab spots measured by RPI. The association curves measured on different spots of p24(c)Ab (*Upper*) and p24(d)Ab (*Lower*) for different concentrations of p24Ag in incubation buffer (*Left*) and in 1:10 dilution of bovine fetal serum (*Right*) are shown. From their exponential fits (red lines), the rates reported as blue circles (*Upper Left*) and cyan circles (*Upper Right*) in Fig. 3*F* and as orange down triangles (*Lower Left*) and open red circles (*Lower Right*) in Fig. 3*G* are obtained.

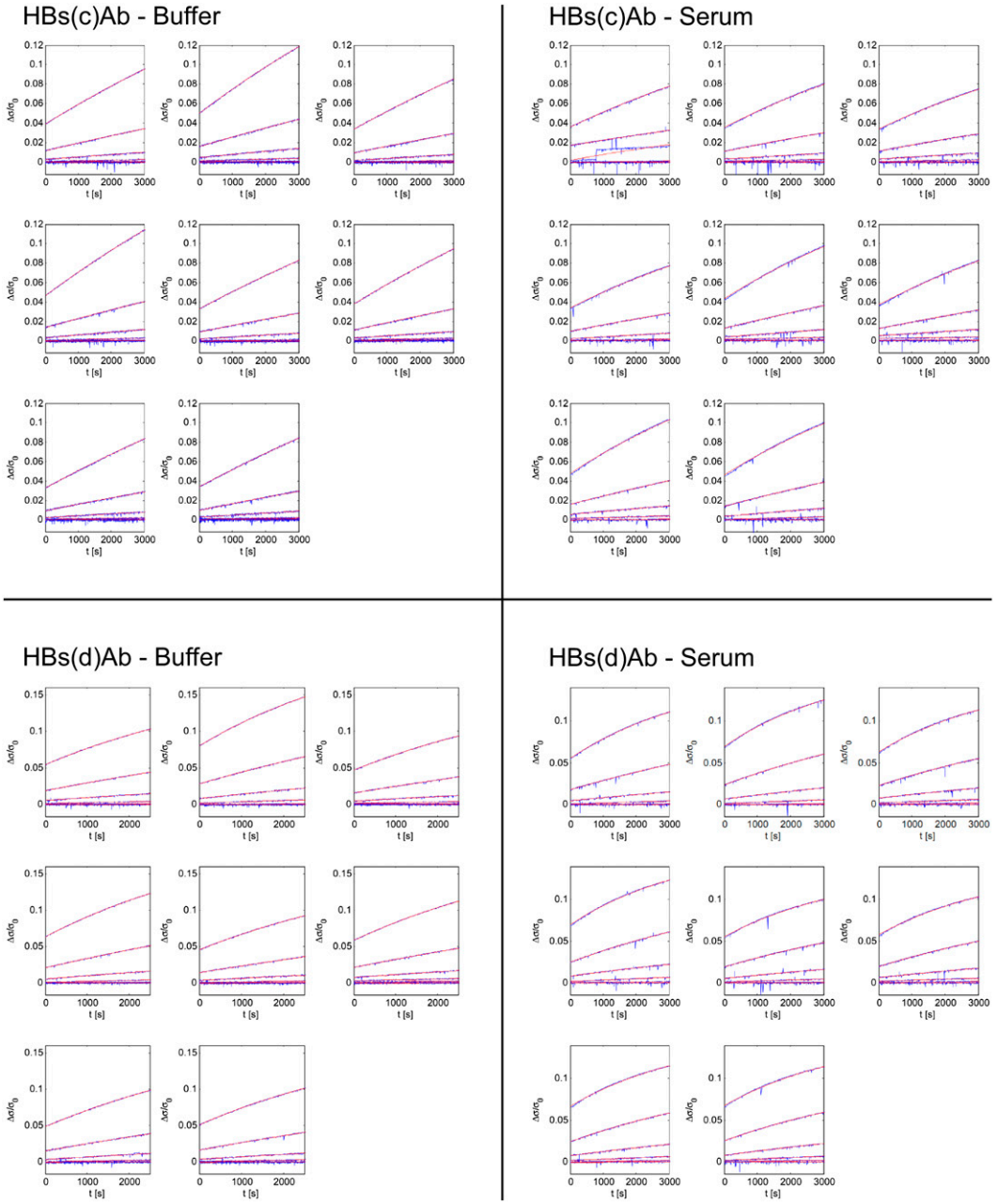

Fig. S4. Binding curves of HBsAg on HBs(c)Ab and HBs(d)Ab spots measured by RPI. The association curves measured on different spots of HBs(c)Ab (*Upper*) and HBs(d)Ab (*Lower*) for different concentrations of HBsAg in incubation buffer (*Left*) and in 1:10 dilution of bovine fetal serum (*Right*) are shown. From their exponential fits (red lines), the rates reported as solid red circles (*Upper Left*), open orange circles (*Upper Right*), solid purple circles (*Lower Left*), and open magenta circles (*Lower Right*) in Fig. 3*F* are obtained.

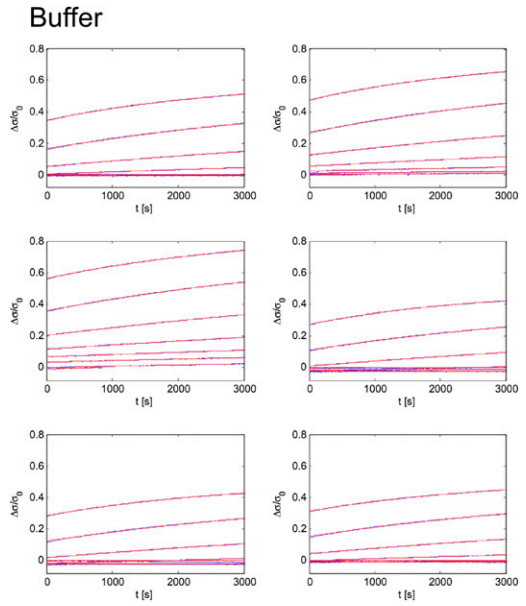

Fig. S5. Binding curves of anti-mouse IgG/mouse IgG interaction measured by RPI. The association curves measured on different spots of anti-mouse IgG for different concentrations of mouse IgG in incubation buffer are shown. From their exponential fits (red lines), the rates reported as solid blue circles in Fig. 4 are obtained. The initial slope of the fitting curve is reported as open violet circles in Fig. 4.

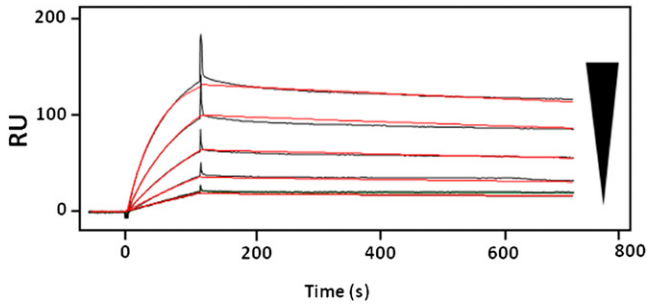

Fig. S6. SPR analysis of the p24(d)Ab/p24Ag interaction. Shown is overlay of blank-subtracted sensorgrams showing the binding of p24Ag (25, 50, 100, 200, and 400 nM from bottom to top) to the CM5 sensorchip containing the antibody. Black lines represent the experimental data. Red lines represent the fit, whose χ^2 was equal to 12.2 (1).

1. Khalifa MB, Choulier L, Lortat-Jacob H, Altschuh D, Vernet T (2001) BIACORE data processing: An evaluation of the global fitting procedure. *Anal Biochem* 293(2):194–203.

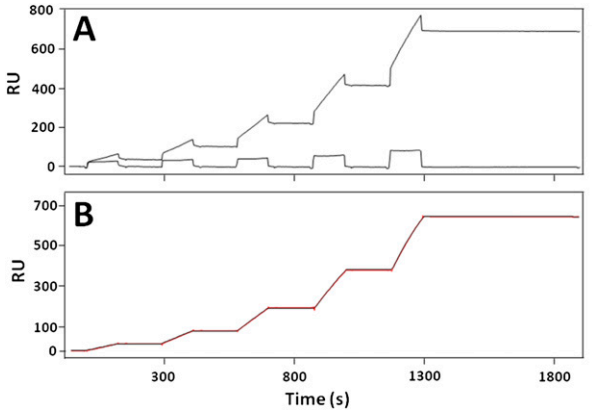

Fig. S7. SPR analysis of the HBs(c)Ab/HBsAg interaction. (*A*) Single-cycle kinetic showing the binding of HBsAg (50, 100, 200, 400, and 800 nM from left to right) to a CM3 sensorchip without (lower sensorgram) or with immobilized HBs(c)Ab antibody (upper sensorgram). (*B*) Blank-subtracted sensorgrams showing the analysis performed above. Black lines represent the experimental data. Red lines represent the fit, whose χ^2 was equal to 3.6 (1).

1. Khalifa MB, Choulier L, Lortat-Jacob H, Altschuh D, Vernet T (2001) BIACORE data processing: An evaluation of the global fitting procedure. *Anal Biochem* 293(2):194–203.

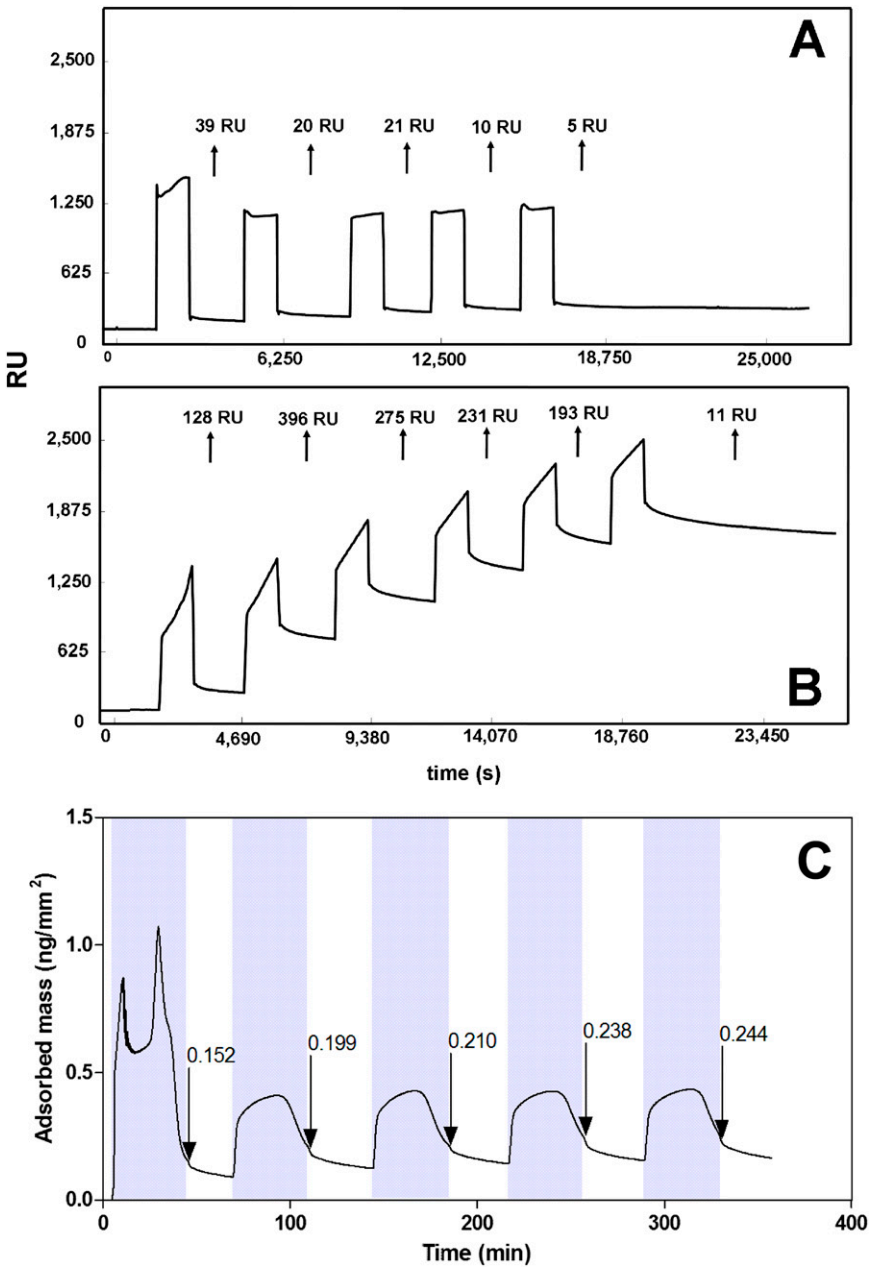

Fig. S8. Serum adsorption to SPR and DPI sensorchips. (*A*) FBS diluted 1:10 in running buffer was repeatedly injected over the sensorchip coated with the copoly(DMA-NAS-MAPS) that was then washed with running buffer to allow the dissociation of adsorbed material. Arrows indicate the amount of serum components (in RU) that remained adsorbed to sensorchips after every injection and washing. (*B*) The experiment reported in *A* was repeated for a commercial sensorchip coated with CM5 carboxyl-methyl-dextran. (*C*) Measurement of the mass increase on a surface coated by copoly(DMA-NAS-MAPS) upon injections of serum diluted in incubation buffer (gray areas). The values of adhering mass at the end of the injections, measured after the instrumental transients, are indicated by the arrows.

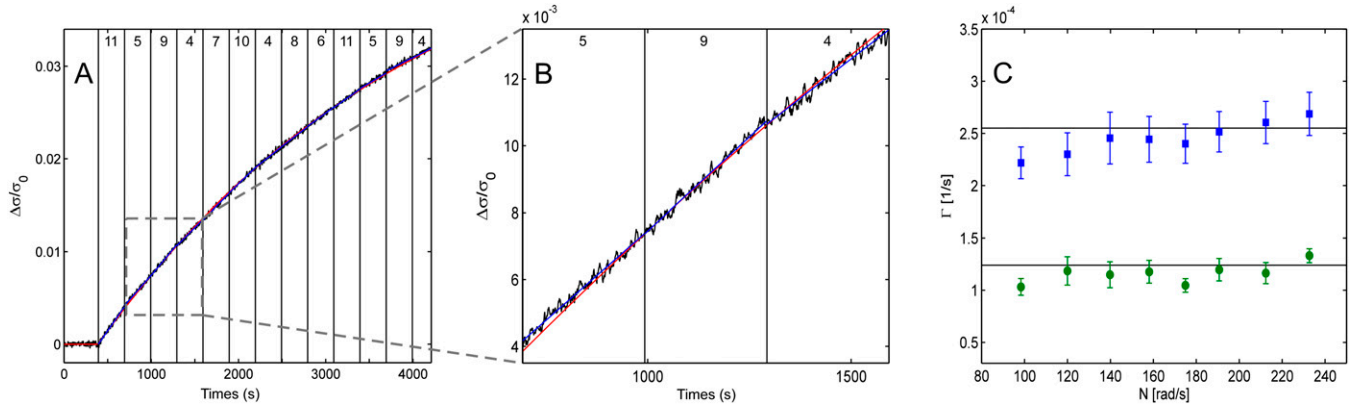

Fig. S9. Effect of the stirring speed on the binding rates measured by RPI. (*A*) The normalized mass adhering on a spot of p24(d)Ab after the addition of 22.7 ng/mL of p24Ag in incubation buffer was measured (black line) while changing the rotational speed of the magnetic stirrer. The vertical black lines indicate the time at which the stirring speed was changed and the reported numbers represent the notch number of the stirrer driver. The corresponding rotational speeds, obtained by measuring the frequency of the fluctuations of the light scattered by the magnetic bar when directly illuminated by a laser source, are 98.4, 120.0, 139.8, 158.1, 175.0, 190.7, 212.4, and, 232.7 rad/s for notch numbers 4, 5, 6, 7, 8, 9, 10, and 11, respectively. The red line represents a single exponential fit to the whole curve, yielding a rate of 2.5×10^{-4} s^{-1}. The blue curves are independent exponential fits, with constrained asymptotic values, of the corresponding curve fragments at constant rotational speed, from which the rates reported in *C* are obtained. (*B*) Magnification of the region of *A* enclosed by the gray dashed box. (*C*) Binding rates as a function of the stirrer rotational speed obtained from the fits (blue lines) of the different fragments of the binding curve on p24(d)Ab spots reported in *A* (blue squares) and from an analogous analysis performed on p24(c)Ab spots (green circles). Error bars indicates the SD of the rates measured from five spots. The horizontal black lines represent the corresponding rates extracted from the fit of the whole binding curves.

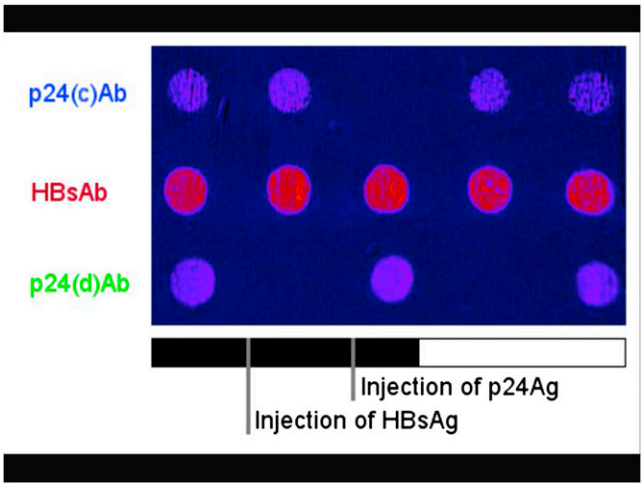

Movie S1. Sequence of difference images of the sensing surface of the prism acquired while adding a solution containing the target molecules to the cuvette. Multiple spots of antibodies p24(c)Ab, HBsAb, and p24(d)Ab are placed in rows, as shown by the labels. The times of addition of the target molecules HBsAg and p24Ag to a concentration of 50 ng/mL are indicated in the progress bar. A reference image, acquired at the beginning of the experiment, before the addition of the targets in solution, has been subtracted from each of the following images. Each pixel records the increase of the local reflectivity over time as more molecules adhere to the surface. The brightness of the images has been rendered with false colors to make variations more visible.

Movie S1